Microwave Probe Based on an Inverted Microstrip Line for Broadband Electron Paramagnetic Resonance Spectroscopy

Selina Eckel, *Graduate Student Member, IEEE*, Matthias Oliver Beck, and Ahmet Çağrı Ulusoy, *Senior Member, IEEE*

***Abstract*—This work presents a broadband inverted microstrip line (IMSL) as a microwave probe for electron paramagnetic resonance (EPR) spectroscopy, a technique used to detect unpaired electron spins in biological and chemical samples. The IMSL geometry enables sample placement in the most homogeneous region of the microwave magnetic field, overcoming limitations of standard coplanar waveguide (CPW) and microstrip line (MSL) probes. Simulated and measured S-parameters confirm broadband operation up to 67 GHz. Improved field homogeneity relative to MSLs is demonstrated by a reduced coefficient of variation of the simulated magnetic field and by EPR measurements showing signal amplitudes independent of sample orientation. The IMSL geometry offers a compact microwave probe with straightforward fabrication for broadband EPR sensing in biological and healthcare applications.**

***Index Terms*—Electron paramagnetic resonance (EPR), inverted microstrip line (IMSL), magnetic-field homogeneity, transmission line (TL).**

I. Introduction

MAGNETIC resonance spectroscopy is a powerful, noninvasive technique for studying molecular structure and dynamics of biological and chemical samples. A subcategory, electron paramagnetic resonance (EPR), enables the study of paramagnetic systems containing unpaired electrons [1]. In biomedical applications, EPR is used, for example, in protein studies, cancer diagnostics, and oxygen monitoring [2], [3], [4].

A fundamental property of the electron is its magnetic moment, which arises from its intrinsic spin. Due to the two possible spin states of the electron ($S = \pm 1/2$), the energies split into two levels in an external magnetic-field B_0

$$E_{\pm 1/2} = \pm \frac{1}{2} g \mu_\mathrm{B} B_0 \tag{1}$$

known as the electronic Zeeman levels, where g is the g-factor, and μ_B is the Bohr magneton. Transitions between these levels occur when the Zeeman splitting matches the photon energy of an applied microwave radiation

$$\Delta E = g \mu_\mathrm{B} B_0 = h f_0 \tag{2}$$

and when the oscillating magnetic field of that microwave radiation, $\vec{B}_1$, is oriented perpendicular to B_0. At resonance, energy is absorbed by the sample and detected as a peak in the EPR spectrum [1]. In this work, this resonance condition serves as the basis for signal detection, while the focus is on the experimental implementation rather than on the analysis of spin energy levels.

In real systems, interactions of the unpaired electron with nearby nuclear or electron spins can give rise to multiple absorption peaks in the EPR spectrum. Measurements at multiple frequencies can provide additional insight into these transitions. While conventional EPR experiments employ resonators operating at fixed frequencies [5], transmission lines (TLs) enable measurements over a wide frequency range, in this work up to 67 GHz, thereby facilitating frequency-resolved EPR measurements [6].

Several broadband EPR probes based on coplanar waveguides (CPW) or microstrip lines (MSL) demonstrate this capability [7], [8], [9]. For continuous-wave EPR, maximizing $\vec{B}_1$ is often the main objective because it increases the detectable signal amplitude. However, for quantitative or pulsed EPR, $\vec{B}_1$ homogeneity becomes equally critical. Field inhomogeneities cause errors in spin counting [10], inaccurate relaxation times [11], or nonuniform flip angles in pulsed EPR [12].

Because the magnetic field above CPW and MSL structures is strongly inhomogeneous, we propose an inverted MSL (IMSL) geometry. Although IMSL structures have found applications in tunable liquid–crystal (LC) devices [13], [14], imaging resonators [15], and gap-waveguide systems [16], their use for EPR has not been explored in detail. Here, we demonstrate that an IMSL can be employed to realize a broadband EPR probe with improved $\vec{B}_1$ homogeneity. In the remainder of this work, the microwave magnetic field is evaluated in terms of $\vec{H}_1$, as $\vec{B}_1$ is proportional to $\vec{H}_1$ for magnetically linear materials with spatially uniform μ_r [17].

II. Design and Field Distribution of the IMSL

Fig. 1(a) illustrates the IMSL cross section in the xy plane, where w denotes the signal width. The substrate is characterized by its height h and dielectric constant ε_r. In this configuration, the signal conductor is placed beneath the substrate, while the ground plane is separated by an air-gap h_G. Fig. 2 shows the simulated microwave magnetic-field lines of $\vec{H}_1$ for the IMSL at $f_0 = 34.8$ GHz. The external magnetic-field B_0 is applied along the y-axis, such that only the $H_{1,x}$ component contributes to the EPR excitation. As a reference, the magnetic-field lines of an MSL are also shown, and Fig. 1(b) illustrates its cross section. The IMSL enables

Received 31 March 2026; accepted 3 April 2026. This work was supported by German Research Foundation under Grant CRC 1527. *(Corresponding author: Selina Eckel.)*

The authors are with the Institute of Radio Frequency Engineering and Electronics, Karlsruhe Institute of Technology, 76131 Karlsruhe, Germany (e-mail: selina.eckel@kit.edu; uekik@student.kit.edu; cagri.ulusoy@kit.edu).

This article was presented at the IEEE MTT-S International Microwave Symposium (IMS2026), Boston, MA, USA, June 7–12, 2026.

Digital Object Identifier 10.1109/LMWT.2026.3682570

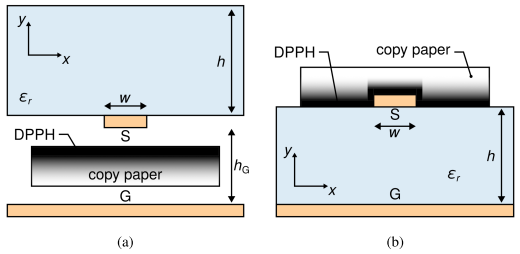

Fig. 1. Cross sections of (a) IMSL and (b) MSL in the xy plane. As the EPR sample, a DPPH-coated (highlighted in black) copy paper is used. The shown position corresponds to the reference sample position in the EPR measurements shown in Fig. 7.

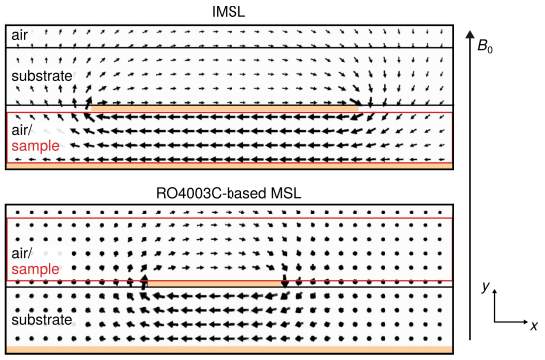

Fig. 2. Simulated magnetic-field lines of the IMSL and the RO4003C-based MSL at f_0 = 34.8 GHz. The size of the arrows scales with the field strength.

sample placement in a homogeneous region of $\vec{H}_1$ between the signal (S) and ground (G) plane, due to the field being confined between the conductors, which is not accessible in the MSL. The accessible region above the MSL exhibits a more inhomogeneous field distribution.

As the field homogeneity is primarily determined by the TL geometry, the IMSL is optimized to achieve a high field strength, since this leads to a stronger EPR signal. The IMSL prototype is designed to have an air gap of h_G = 200 μm, which represents a compromise between sample accessibility and magnetic-field strength. The signal conductor has a width of w = 925 μm, and the microwave substrate is Rogers RO4003C (ε_r = 3.43, h = 200 μm), resulting in Z_0 = 50 Ω. The magnetic field is mainly determined by the region between the signal line and ground plane, so the substrate material has only a minor influence on the overall $\vec{H}_1$ strength, in contrast to the MSL. Simulations show that increasing the dielectric constant slightly enhances $\vec{H}_1$, but the effect is small. Consequently, RO4003C is selected over alumina due to its easier handling and lower fabrication complexity. The probe is designed for an operational bandwidth of up to 67 GHz.

The IMSL design consists of four separate pieces: two coaxial connector-to-MSL transitions, the MSL-IMSL transition, and the copper ground plate (thickness 200 μm), which also provides mechanical stability. Compared to MSL and CPW, the transition from the connector to the IMSL is more challenging, since the substrate needs to be flipped while the position of the conductors is not changed. The cross section of the different transitions in the yz plane is shown in Fig. 3. The connector-to-MSL transition follows the design guidelines as described in our previous work [18]. The connectors are mounted on a GSG pad, which is transformed into an MSL by tapering the ground pads that are gradually terminated. To

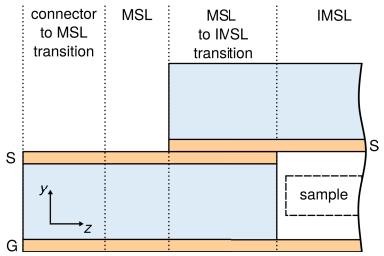

Fig. 3. Cross section of the IMSL in the yz plane illustrating the transition from the connector to the MSL and further to the IMSL.

realize the MSL-IMSL transition, the substrate height of the MSL is intentionally chosen to match the air-gap size, allowing the MSL substrate to transition naturally into the air region of the IMSL. This design ensures a seamless mechanical and electromagnetic continuation between both regions without additional support or height correction. The MSL-IMSL transition spans 4 mm, with the MSL width (w_{MSL} = 410 μm) tapered to the IMSL width (w = 925 μm) for a smooth impedance profile. The transition concept is inspired by [14], employing a different transition geometry and an adaptation of the dimensions for EPR rather than LC applications. The fully assembled IMSL probe is shown in Fig. 4(a). The IMSL is mounted above the MSL using four screws per side. Applying soldering paste at the transition is also tested but shows no measurable improvement in the transmission coefficient S_{21}. Fig. 4(b) presents the unfolded IMSL, where the upper part displays the mounted connector-to-MSL transitions on the ground plane, and the lower part shows the MSL-to-IMSL transition. The complete probe, without connectors, measures 28 × 12.8 mm. For comparison, the IMSL is evaluated against two MSL reference probes. Photographs of the two fabricated MSL probes are shown in Fig. 4(c) and (d). To provide a meaningful comparison, each MSL design serves a distinct purpose.

1) A RO4003C-based MSL (h = 200 μm, w = 440 μm, Z_0 = 50 Ω), which serves as a direct counterpart to the IMSL on the same substrate.
2) An alumina-based MSL (ε_r = 9.9, h = 250 μm, w = 235 μm) serves as a comparison to a higher performing conventional design, as a higher ε_r leads to a stronger microwave magnetic field [18], independent of the specific field component.

Both MSLs have dimensions 17.8 × 12.8 mm.

III. Experimental Results

The simulated and measured transmission coefficient S_{21} of the IMSL are shown in Fig. 5. The simulation includes a connector offset of 100 μm and a metal surface roughness of 2 μm. Overall, the simulated and measured responses follow the same general trend. The measurement, however, exhibits slightly higher insertion losses and shows two additional dips near 12 and 29 GHz, which are attributed to assembly related tolerances (e.g., air-gap height and alignment variations). These effects primarily influence the transmission efficiency rather than the underlying $\vec{H}_1$ field distribution in the sample region and are therefore not expected to significantly affect the EPR response within the narrow resonance bandwidth. Fig. 5 also shows the measured S_{21} results for both MSL structures. The slightly higher insertion loss of the IMSL,

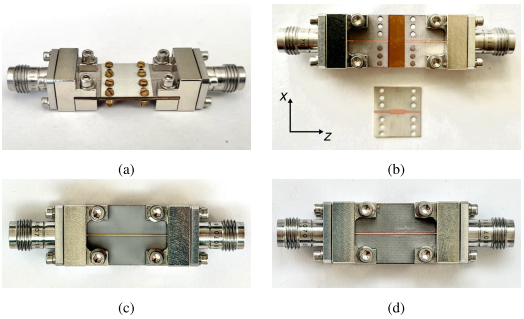

Fig. 4. Photograph of the fabricated TLs. The IMSL is shown in (a) as the fully assembled structure and (b) in its unfolded configuration. The MSL is fabricated on two different substrates (c) alumina and (d) RO4003C.

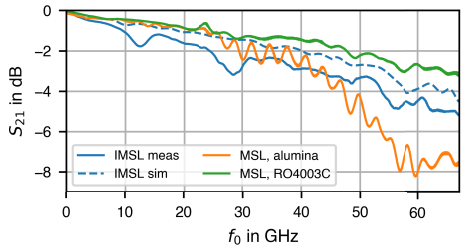

Fig. 5. Measured and simulated transmission coefficient of the IMSL and measured transmission coefficient of both MSL designs.

compared with the RO4003C-based MSL, is mainly due to the longer structure and additional transitions. For frequencies higher than approximately 45 GHz, the IMSL exhibits a lower insertion loss than the alumina-based MSL, as high-permittivity substrates are more susceptible to substrate-mode excitation, resulting in increased losses [17].

EPR measurements are performed using the setup shown in Fig. 6. A detailed description of the measurement procedure is provided in [18] and is briefly revisited here to outline the main operating principle. A microwave signal of frequency f_0 is fed into the TL probe, which is positioned inside a custom-built, 3-D-printed Helmholtz modulation coil placed within an electromagnet. As described above, the external magnetic-field B_0 is oriented along the y-axis. The structures are positioned on their edge such that the $H_{1,x}$ component is perpendicular to B_0. The lock-in amplifier drives the modulation coils at a frequency f_m and amplitude B_m, generating a sinusoidal modulation of the magnetic field. This modulation causes a corresponding modulation of the EPR absorption. The detector demodulates this signal, while the lock-in amplifier down-converts it to direct current and filters it with a time constant τ. The final EPR signal is measured as a voltage. The input power $P_0 = 4.2$ dBm is calibrated up to the input of the microwave probe, and the remaining parameters are $f_\mathrm{m} = 20$ kHz, $B_\mathrm{m} = 60\ \mu$T, and $\tau = 70$ ms.

The test sample consists of a strip of standard 80-g/m^2 copy paper with a thickness of approximately 100 μm, which is soaked in a 2,2-diphenyl-1-picrylhydrazyl (DPPH) acetone solution following [9]. The thin paper acts as the supporting base, while DPPH is the EPR-active material and exhibits a single EPR resonance line. It is a standard radical used in EPR [5]. After soaking, the paper remains in the vessel while the acetone evaporates, leaving a thin DPPH film on its surface. During drying, the side of the paper in contact with the bottom of the vessel becomes only lightly coated, while the opposite

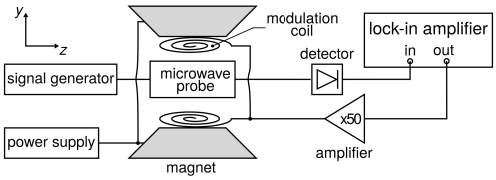

Fig. 6. Broadband EPR measurement setup consisting of commercial measurement instruments and the designed TL microwave probes [18].

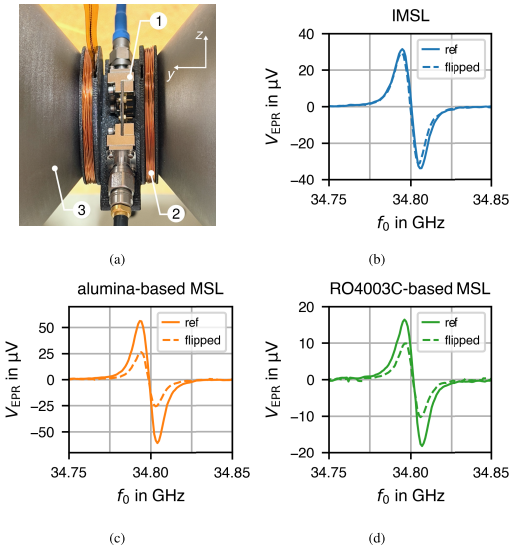

Fig. 7. (a) Photograph of the IMSL (1), inside the modulation coil (2), and between the poles of the electromagnet (3). EPR measurements for both sample orientations using (b) IMSL, (c) RO4003C-based MSL, and (d) alumina-based MSL. The reference orientation corresponds to the DPPH-coated side facing the signal line (see Fig. 1).

side develops a homogeneous DPPH layer. The coated side is easily identifiable, as DPPH forms a dark purple, almost black film, whereas the opposite side appears much lighter. The prepared DPPH strip has dimensions 2.5 × 12.8 mm, matching the width of the TL structures.

This sample design enables a straightforward test of $\vec{H}_1$ homogeneity. If the TL probe produces a homogeneous $\vec{H}_1$ field across the sample region, the EPR signal amplitude should be independent of the sample orientation, for example, which side of the sample faces the signal line. To evaluate this, the sample is measured in two orientations: first with the DPPH-rich side facing the signal line (illustrated in Fig. 1), and then flipped so that this side faces the ground plane.

Fig. 7 compares representative EPR results obtained at an external magnetic-field strength of $B_0 = 1.241$ T with swept microwave frequency. For DPPH ($g = 2.0037$ [1]), (2) gives a resonance frequency of $f_0 = 34.8$ GHz at this field, where all shown EPR spectra exhibit a peak at this expected frequency. As a result of the magnetic-field modulation, the measured signal represents the derivative of the absorption spectrum and exhibits the expected single-line shape of DPPH [1], [5]. For the IMSL, the spectra of both sample orientations are nearly identical, confirming a uniform $\vec{H}_1$ across the sample. In contrast, both MSLs show a significant reduction in peak-to-peak amplitude when flipped, especially the alumina-based MSL, consistent with its stronger field confinement. These results demonstrate that the IMSL provides a more uniform $\vec{H}_1$ distribution across the sample region compared to both MSL reference structures.

Based on simulation results, the IMSL yields a coefficient of variation (standard deviation divided by mean) of 17% in $H_{1,x}$, compared to 41% for the MSL, quantitatively confirming the improved field homogeneity of the IMSL. This evaluation considers only values within 80% of the respective maximum magnetic-field amplitude (IMSL: 270 A/m, MSL: 317 A/m).

IV. Discussion and Conclusion

This work demonstrates that an IMSL can be employed as a broadband EPR probe providing improved microwave magnetic-field homogeneity compared to conventional MSL structures, as confirmed by electromagnetic simulations and orientation-dependent EPR measurements.

An alternative approach to improving field homogeneity employs MSL probes with an etched substrate cavity [9]. While this design enables access to a more uniform field region within the dielectric, it requires lithographic fabrication and access to specialized facilities. In contrast, the IMSL achieves comparable field uniformity without such demanding manufacturing steps.

The presented results establish the IMSL as a compact microwave probe suitable for homogeneous, broadband EPR sensing in biological and healthcare applications, while maintaining a straightforward assembly and implementation.

Acknowledgment

The authors thank Luca Valenziano, Thorsten Fux, Matthias Tazib, and Henning Poensgen for their support at our institute, and Charlie Jackson for fruitful discussions on IMSLs.

References

[1] J. A. Weil and J. R. Bolton, *Electron Paramagnetic Resonance: Elementary Theory and Practical Applications*. Hoboken, NJ, USA: Wiley, 2007.

[2] M. Margittai and R. Langen, "Spin labeling analysis of amyloids and other protein aggregates," *Methods Enzymol.*, vol. 413, pp. 122–139, 2006.

[3] M. Zdybel, E. Chodurek, and B. Pilawa, "Application of EPR spectroscopy to determine the influence of simvastatin concentration on free radicals in A-375 human melanoma malignum cells," *Toxicol. Vitro*, vol. 61, Dec. 2019, Art. no. 104620.

[4] A. Matsumoto et al., "Absolute oxygen tension (pO_2) in murine fatty and muscle tissue as determined by EPR," *Magn. Reson. Med.*, vol. 54, no. 6, pp. 1530–1535, Dec. 2005.

[5] G. R. Eaton, S. S. Eaton, D. P. Barr, and R. T. Weber, *Quantitative EPR*. Cham, Switzerland: Springer, 2010.

[6] S. K. Misra, *Multifrequency Electron Paramagnetic Resonance: Theory and Applications*. Hoboken, NJ, USA: Wiley, 2011.

[7] Y. Wiemann et al., "Observing electron spin resonance between 0.1 and 67 GHz at temperatures between 50 mK and 300 K using broadband metallic coplanar waveguides," *Appl. Phys. Lett.*, vol. 106, no. 19, May 2015, Art. no. 193505.

[8] Z. Chen, J. Sun, and P. Wang, "Broadband ESR spectroscopy with a tunable interferometer," *IEEE Trans. Magn.*, vol. 53, no. 8, pp. 1–9, Aug. 2017.

[9] P. R. Shrestha et al., "Nonresonant transmission line probe for sensitive interferometric electron spin resonance detection," *Anal. Chem.*, vol. 91, no. 17, pp. 11108–11115, Sep. 2019.

[10] V. N. Syryamina, A. G. Matveeva, Y. V. Vasiliev, A. Savitsky, and Y. A. Grishin, "Improving B1 field homogeneity in dielectric tube resonators for EPR spectroscopy via controlled shaping of the dielectric insert," *J. Magn. Reson.*, vol. 311, Feb. 2020, Art. no. 106685.

[11] P. Fajer and D. Marsh, "Microwave and modulation field inhomogeneities and the effect of cavity Q in saturation transfer ESR spectra. Dependence on sample size," *J. Magn. Reson.*, vol. 49, no. 2, pp. 212–224, Sep. 1982.

[12] J. S. Hyde, J. W. Sidabras, and R. R. Mett, "Uniform field resonators for EPR spectroscopy: A review," *Cell Biochemistry Biophys.*, vol. 77, no. 1, pp. 3–14, Mar. 2019.

[13] D. C. Zografopoulos, A. Ferraro, and R. Beccherelli, "Liquid-crystal high-frequency microwave technology: Materials and characterization," *Adv. Mater. Technol.*, vol. 4, no. 2, Feb. 2019, Art. no. 1800447.

[14] P. Deo, D. Mirshekar-Syahkal, L. Seddon, S. E. Day, and F. A. Fernandez, "Microstrip device for broadband (15–65 GHz) measurement of dielectric properties of nematic liquid crystals," *IEEE Trans. Microw. Theory Techn.*, vol. 63, no. 4, pp. 1388–1398, Apr. 2015.

[15] X. Zhang, K. Ugurbil, R. Sainati, and W. Chen, "An inverted-microstrip resonator for human head proton MR imaging at 7 Tesla," *IEEE Trans. Biomed. Eng.*, vol. 52, no. 3, pp. 495–504, Mar. 2005.

[16] Z.-H. Shi, F. Wei, L. Yang, and R. Gómez-García, "High-selectivity inverted microstrip gap waveguide bandpass filter using hybrid cavity and stub-loaded ring resonant modes," *IEEE Trans. Circuits Syst. II, Exp. Briefs*, vol. 71, no. 1, pp. 146–150, Jan. 2024.

[17] D. M. Pozar, *Microwave Engineering*, 4th ed., Hoboken, NJ, USA: Wiley, 2021.

[18] S. Eckel, J. Nagel, M. Jouda, J. G. Korvink, and A. Ç. Ulusoy, "Design of planar transmission line microwave probes for broadband EPR spectroscopy," *J. Magn. Reson.*, vol. 374, May 2025, Art. no. 107866.